



High stretchability, strength, and toughness of living cells enabled by hyperelastic vimentin intermediate filaments

Jiliang Hu^a, Yiwei Li^a, Yukun Hao^a, Tianqi Zheng^a, Satish K. Gupta^a, German Alberto Parada^b, Huayin Wu^c, Shaoting Lin^a, Shida Wang^a, Xuanhe Zhao^{a,d}, Robert D. Goldman^e, Shengqiang Cai^f, and Ming Guo^{a,1}

^aDepartment of Mechanical Engineering, Massachusetts Institute of Technology, Cambridge, MA 02139; ^bDepartment of Chemical Engineering, Massachusetts Institute of Technology, Cambridge, MA 02139; ^cSchool of Engineering and Applied Sciences, Harvard University, Cambridge, MA 02138; ^dDepartment of Civil and Environmental Engineering, Massachusetts Institute of Technology, Cambridge, MA 02139; ^eDepartment of Cell and Molecular Biology, Northwestern University Feinberg School of Medicine, Chicago, IL 60611; and ^fDepartment of Mechanical and Aerospace Engineering, University of California San Diego, La Jolla, CA 92093

Edited by Jennifer Lippincott-Schwartz, Janelia Farm Research Campus, Ashburn, VA, and approved July 23, 2019 (received for review March 6, 2019)

In many developmental and pathological processes, including cellular migration during normal development and invasion in cancer metastasis, cells are required to withstand severe deformations. The structural integrity of eukaryotic cells under small deformations has been known to depend on the cytoskeleton including actin filaments (F-actin), microtubules (MT), and intermediate filaments (IFs). However, it remains unclear how cells resist severe deformations since both F-actin and microtubules yield or disassemble under moderate strains. Using vimentin containing IFs (VIFs) as a model for studying the large family of IF proteins, we demonstrate that they dominate cytoplasmic mechanics and maintain cell viability at large deformations. Our results show that cytoskeletal VIFs form a stretchable, hyperelastic network in living cells. This network works synergistically with other cytoplasmic components, substantially enhancing the strength, stretchability, resilience, and toughness of cells. Moreover, we find the hyperelastic VIF network, together with other quickly recoverable cytoskeletal components, forms a mechanically robust structure which can mechanically recover after damage.

vimentin | intermediate filament | cytoskeleton | cytoplasm | cell mechanics

Mesenchymal cells such as fibroblasts play central roles in many physiological processes including the epithelial to mesenchymal transition (EMT) that takes place during normal embryonic development, in cancer metastasis, and in wound healing (1, 2). During these physiological processes, mesenchymal cells experience severe deformations as they engage in the migratory and invasive activities associated with these processes (3), highlighting the importance for cells to maintain mechanical integrity under large deformations. Recent studies have emphasized the importance of nuclear envelope rupture and repair mechanisms in limiting DNA damage during mechanical stress (4, 5). In contrast, the mechanisms involved in protecting the remaining cytoplasm and its constituent organelles against severe deformations remain unclear.

The ability of eukaryotic cells to resist deformation depends on the cytoskeleton, an interconnected network of biopolymers including F-actin, MT, and IFs (6). Previous in vitro work has demonstrated that both F-actin and MT structures yield or disassemble at moderate strains (20 and 60%, respectively) (7), suggesting that they cannot maintain the mechanical integrity and resilience of the cytoplasm at the even larger strains which take place in the physiological processes mentioned above. Therefore, it has been hypothesized that cytoplasmic IFs may play an important role in maintaining the mechanical integrity and resilience of cells, especially under large deformations (8, 9). As a key phenotypic marker of mesenchymal cells, vimentin IFs (VIFs) are known to be critical for regulating cell shape, migration (10), and cytoplasmic stiffness at small deformations (11,

12). However, their structural and mechanical roles in living mesenchymal cells at large deformations remain unknown.

Here we show that VIFs behave as a strain-stiffening hyperelastic network in mesenchymal cells and that they determine cellular strength, stretchability, resilience, and toughness. VIF networks interconnect with other cytoskeletal networks and effectively disperse local deformations in the cytoplasm, and thus lead to a significant increase in the mechanical energy input required to damage the cytoplasm. Furthermore, the hyperelastic VIF network can dramatically slow down both poroelastic relaxation and viscoelastic relaxation processes in the cytoplasm, which can enhance the mechanical damping capability of the cytoplasm and thus protect organelles against mechanical damage. Our results provide a fundamental insight into the role of cytoskeletal IFs in the maintenance of cell structure, mechanical integrity, and resilience during a variety of key physiological processes.

Results

VIF Networks Dominate Cytoplasmic Mechanics and Maintain Cell Viability under Large Deformations. To study the effect of VIFs in cytoplasmic mechanics, we use wild-type (WT) and vimentin

Significance

Intermediate filaments (IFs) remain the least understood with respect to their functions in mammalian cells even though they have been related to many devastating human diseases. Here we use optical tweezers to perform micromechanical measurements in living cells and in IF enriched cytoskeletons devoid of actin and microtubules. We identify that cytoskeletal vimentin IFs (VIFs) provide cells with a hyperelastic rubber-like network that regulates the essential mechanical properties of mammalian cells including stretchability, strength, resilience, and toughness. We show that VIFs maintain cell integrity and viability under conditions involving extreme deformations. We further show that the stretchy VIF network can effectively disperse locally induced mechanical stress to larger regions within individual cells, enabling the dissipation of energy throughout a cell.

Author contributions: J.H. and M.G. designed research; J.H., Y.L., Y.H., and T.Z. performed research; Y.L., Y.H., T.Z., S.K.G., G.A.P., H.W., S.L., X.Z., R.D.G., and S.C. contributed new reagents/analytic tools; J.H., Y.L., Y.H., and S.W. analyzed data; M.G. supervised the project; and J.H., R.D.G., S.C., and M.G. wrote the paper.

The authors declare no conflict of interest.

This article is a PNAS Direct Submission.

Published under the PNAS license.

¹To whom correspondence may be addressed. Email: guom@mit.edu.

This article contains supporting information online at www.pnas.org/lookup/suppl/doi:10.1073/pnas.1903890116/-DCSupplemental.

Published online August 13, 2019.

null ($Vim^{-/-}$) mouse embryonic fibroblasts (mEFs); these cells have been shown to have extensive arrays of other cytoskeletal systems such as microtubules and F-actin as described in previous studies (11, 13) (SI Appendix, Figs. S1–S3). To demonstrate the importance of VIFs in cells undergoing large deformations, we encapsulate living WT and $Vim^{-/-}$ mEFs in biocompatible hydrogels composed of alginate and polyethylene glycol (PEG). The PEG–alginate hydrogel is both tough and highly stretchable; therefore, mEFs encapsulated in this 3D matrix can be highly deformed by stretching the hydrogel (14). Hydrogels with encapsulated mEFs are subjected to 5 different stretching regimes ranging from 0 to 300%, and cell viability is determined by carrying out cell viability (live/dead) assays (Fig. 1A and SI Appendix, Fig. S4). We find that WT mEFs maintain a high viability (~90%) under stretch, while the viability of $Vim^{-/-}$ mEFs decreases significantly as the strain increases (Fig. 1B). This result reveals a key role of VIFs in maintaining cell viability under large deformation.

To understand these findings, we study how VIFs impact the structural integrity and mechanical behavior of living cells. To do so, polystyrene beads (diameter $a = 1 \mu\text{m}$) are introduced into living WT and $Vim^{-/-}$ mEFs through endocytosis (SI Appendix, Fig. S5). These beads are much larger than the typical cytoskeleton mesh size (~50 nm) and thus can probe the cytoplasm as a continuous medium (15–18). To probe the cytoplasmic mechanics, we use optical tweezers to drag a bead unidirectionally

toward the nucleus with a constant speed of $1.0 \mu\text{m/s}$, as illustrated in Fig. 1E (19). The resultant resistant force (F) from the surrounding cytoplasmic structures continuously increases with the displacement (X) of the bead until a peak force is reached, after which the material yields (Fig. 1F). The normalized peak force (peak F/S , where S is the bead cross-sectional area) and the normalized displacement under peak F/S (defined as peak X/a) are determined in order to characterize the cytoplasmic strength and stretchability, respectively (Fig. 1G and H); both peak F/S and peak X/a are significantly larger in WT mEFs than in $Vim^{-/-}$ mEFs, showing that VIFs substantially increase the cytoplasmic strength and stretchability. Moreover, we calculate the extension work density by integrating the normalized force–displacement curve (from $X/a = 0$ to $X/a = 1.2$) to characterize cytoplasmic toughness. The extension work of WT mEFs ($35.7 \pm 8.6 \text{ Pa}$) is about 3 times that of $Vim^{-/-}$ mEFs ($12.1 \pm 4.2 \text{ Pa}$), which indicates that VIFs can significantly improve cytoplasmic toughness.

To further investigate the mechanical properties of cytoplasmic VIF networks, major cellular components including cell membranes, F-actin, and microtubules are extracted from WT mEFs (20) while leaving only the VIF network structure in situ as a ghost cell (SI Appendix, Fig. S2). The VIF network structures seen in live cells are preserved in the ghost cells, as shown in reconstituted 3D images (Fig. 1D and Movie S1). Under small

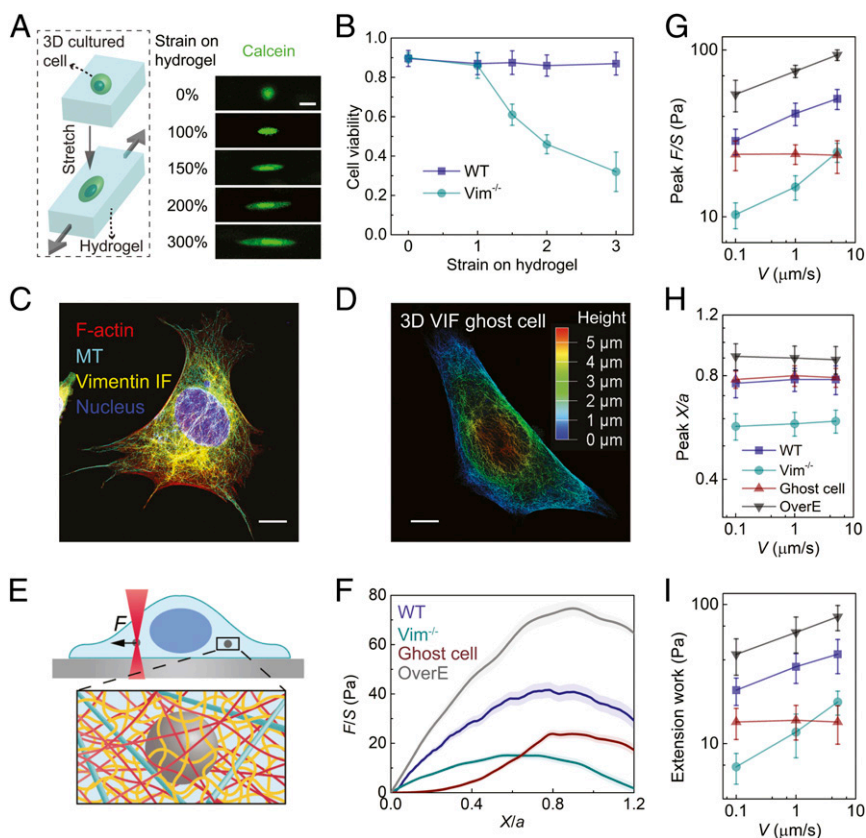


Fig. 1. VIF network maintains cell viability under large deformations and increases the mechanical strength, stretchability, and toughness of the cytoplasm. (A) Cells cultured in 3D PEG–alginate hydrogels are deformed by stretching the hydrogels. Cells are labeled with calcein to visualize cell shape and viability. (Scale bar: $20 \mu\text{m}$.) (B) The viability of WT and $Vim^{-/-}$ mEFs are measured with live/dead assay under various strains for 2 h ($n = 15$). (C) Immunofluorescence image of WT mEF showing the microtubule and vimentin IF cytoskeletons. (Scale bar: $10 \mu\text{m}$.) (D) A 3D microscopic image of VIF in a ghost cell. The color represents height. (Scale bar: $10 \mu\text{m}$.) (E) Schematic of micromechanical measurements in the cytoplasm using optical tweezers. The cytoskeletal mesh size and bead size are not in their actual proportion, just for illustration. (F) Normalized force–displacement curves obtained in cells at $V = 1 \mu\text{m/s}$, from which we calculate peak F/S , peak X/a , and extension work. The semitransparent band around the average curves represents the SE ($n = 20$ cells for each curve). (G–I) The dependence of peak F/S (G), peak X/a (H), and extension work (I) on loading rate in different cells. Error bars represent SD ($n = 20$ cells). These mechanical properties have statistical difference between WT and $Vim^{-/-}$ mEFs and between WT and OverE mEFs ($P < 0.001$ in Student’s t test).

deformations, the resistant force measured by dragging a bead in a ghost cell is lower than that in $Vim^{-/-}$ mEFs at the same displacement (Fig. 1F). However, the force required to further deform the ghost cell exceeds that of $Vim^{-/-}$ mEFs due to the strong strain stiffening behavior of the VIF networks (21); surprisingly, it reaches a peak F/S of 23.8 ± 3.2 Pa, which is markedly larger than that of $Vim^{-/-}$ cells (15.1 ± 2.5 Pa). Indeed, the ghost cell has a similar peak strain (X/a) as that of WT mEFs (Fig. 1H). Moreover, as we depolymerize both F-actin and MTs using pharmacological inhibitors, we find a similar behavior as VIF ghost cells (SI Appendix, Fig. S6). These results show that VIFs determine the mechanical behavior of the cytoplasm under moderate to severe deformations. Furthermore, as we overexpress VIFs in WT mEFs (OverE mEFs), we find that the strength, stretchability, and toughness of the cytoplasm are further enhanced (Fig. 1G–I and SI Appendix, Fig. S7). This critical role of VIFs in enhancing the strength, stretchability, and toughness of the cytoplasm is very important for a variety of physiological processes that involve large cellular deformations, such as those seen in embryonic development and in metastasis.

Cells are additionally known to behave as viscoelastic and poroelastic materials whose mechanical behavior strongly depends on the deformation rate (19, 22, 23). To further characterize the impact of loading rate on the role of VIFs, force–displacement relationships are determined in WT mEFs, $Vim^{-/-}$ mEFs, and VIF ghost cells under a range of loading speeds (0.1 to 5.0 $\mu\text{m/s}$), as shown in SI Appendix, Fig. S8. Interestingly, we find that the peak F/S , peak X/a , and extension work are independent of loading speed in the ghost cell (Fig. 1G–I), suggesting that VIFs can be regarded as a rate-insensitive hyperelastic network with negligible energy dissipation. In contrast, the peak F/S and extension work increase with loading speed in both living WT and $Vim^{-/-}$ mEFs (Fig. 1H and I), reflecting the combined rate-dependent nature of the other cytoskeletal components.

VIF Network Increases the Force Relaxation, Relaxation Time, and Resilience of the Cytoplasm. To further study the effect of VIFs on cytoplasmic rate-dependent behavior, relaxation tests are carried out in cells by applying an instant deformation ($X/a = 0.4$, $V = 100 \mu\text{m/s}$) with a 1- μm -diameter bead using optical tweezers. We then hold the bead and record the corresponding resistant force as a function of time. The resistant force in the VIF ghost cell slightly relaxes (relaxed $F/S = 0.75 \pm 0.40$ Pa) at short time scale ($t < 0.05$ s) and remains at a steady plateau over the experimental time scales employed ($0.05 \text{ s} < t < 10 \text{ s}$) (Fig. 2A–C). The initial force relaxation in the VIF ghost cell at short time scales follows an exponential decay (Fig. 2C, Inset), consistent with our finite element simulation using an isotropic linear poroelastic model as shown in SI Appendix, Fig. S9 (19, 23). Furthermore, using probes of different sizes, we have previously demonstrated that the size-dependent mechanical response measured in the cytoplasm at relatively short time scales quantitatively agrees with the predictions from linear poroelastic model (19). The poroelastic effect in the cytoplasm accounts for the resistance to the flow of soluble/cytosolic materials through porous cytoskeletal structures. Poroelastic fitting [$F/S \sim \exp(-t/t_p)$] of the averaged relaxation curve in the VIF ghost cell yields a poroelastic relaxation time $t_p = 0.028 \pm 0.004$ s, which is consistent with previous measurements in mammalian cells (19, 23). These results suggest that VIF networks act as a porous and hyperelastic meshwork exhibiting negligible viscous effects, which is consistent with macroscopic rheology tests on reconstituted VIF networks (7). In WT and $Vim^{-/-}$ mEFs, the force relaxation curves exhibit an exponential decay followed by a power law decay (Fig. 2C). The initial short-time exponential decay regime and the long-time power law decay regime of the resistant force correspond to poroelastic and viscoelastic relaxations of the cytoplasm, respectively (22–24). Taken together, the results further reveal that the VIF network is hyperelastic but the other cytoplasmic components are viscoelastic, while all of them share an intrinsically porous nature.

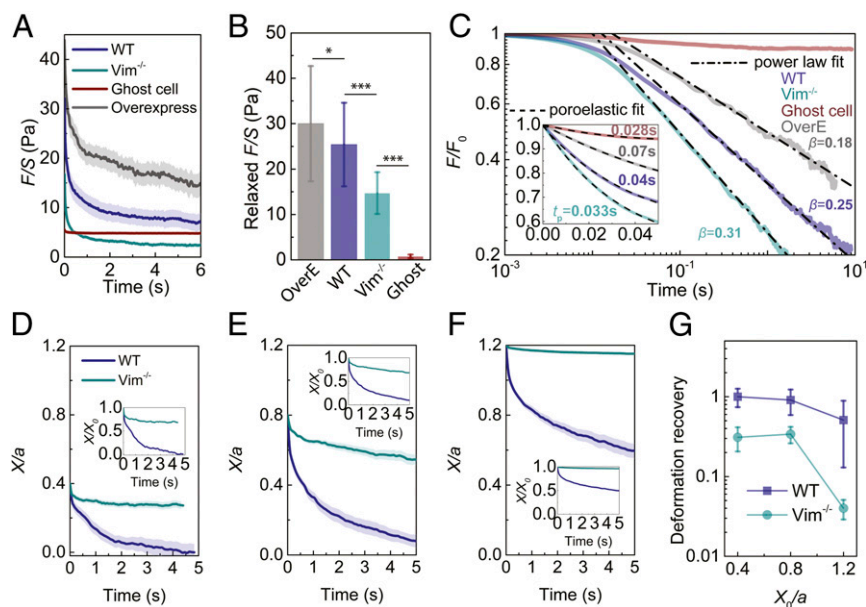


Fig. 2. The elastic VIF network increases the relaxed force, relaxation time, and yielding strain of the cytoplasm. (A) Force relaxation curves of different cells under an instant initial $X/a = 0.4$. The semitransparent band around the average curves represents the SE ($n = 15$ cells for WT and overexpress, $n = 25$ cells for $Vim^{-/-}$ and ghost cell). (B) Comparison of cellular relaxed force, which is defined as the decrease of F/S over the relaxation test. Error bars represent SD ($n = 15$ cells for WT and overexpress, $n = 25$ cells for $Vim^{-/-}$ and ghost cell). (C) Relaxation curves are normalized with initial F_0 at $t = 0$. The curves are fitted with viscoelastic power law decay at long time scales ($0.05 \text{ s} < t < 10 \text{ s}$) and are fitted with poroelastic exponential decay (Inset) at short time scales ($t < 0.05 \text{ s}$). (D–F) Deformation recovery in the cytoplasm of WT and $Vim^{-/-}$ mEFs under different initial normalized displacement ($X_0/a = 0.4$, $X_0/a = 0.8$, and $X_0/a = 1.2$, respectively). The semitransparent band around the average curves represents the SE ($n = 15$ cells for each curve). (G) The cytoplasmic deformation recovery (defined as the recovered deformation over initial deformation) under different initial deformations in WT and $Vim^{-/-}$ mEFs. * $P < 0.05$; *** $P < 0.001$.

The relaxed normalized force (relaxed F/S) is higher in the WT mEFs (25.4 ± 9.2 Pa) than that in the $Vim^{-/-}$ mEFs (14.7 ± 4.6 Pa), as shown in Fig. 2B. Interestingly, the presence of VIFs markedly increases the poroelastic relaxation time in cells; we find that $t_p = 0.042 \pm 0.008$ s in the WT mEFs and 0.033 ± 0.005 s in the $Vim^{-/-}$ mEFs (Fig. 2C, *Inset*). This suggests that VIFs reduce the average cytoplasmic mesh size. Moreover, as we fit the relaxation curves at long time scales ($t > 0.1$ s, as shown in Fig. 2C) to a power law function (23, 24), $F/S \sim t^{-\beta}$, to characterize the viscoelastic relaxation speed of the cytoplasm, we find a lower relaxation speed ($\beta = 0.25 \pm 0.04$) in the WT mEFs compared to the $Vim^{-/-}$ mEFs ($\beta = 0.31 \pm 0.03$). This might be due to friction and other interactions between VIF networks and other cytoskeletal components. Consistently, both the relaxation time and the relaxed force further increase in living mEFs with VIFs overexpressed (OverE), as shown in Fig. 2C. The increased relaxed force and relaxation times in the WT and OverE mEFs, compared with the $Vim^{-/-}$ mEFs, imply that VIF networks can regulate the mechanical damping capacity of the cytoplasm and thereby provide an optimal protection against mechanical stress and damage for organelles while maintaining the structural integrity of cells.

The relaxation test results indicate that VIF networks remain elastic up to deformations of $X/a = 0.4$. To study the yielding strain (the strain limit after which the material exhibits a plastic response) of VIF networks in living cells, we apply different deformations ($X/a = 0.4$ to 1.2) by dragging a 1- μm -diameter bead at 1 $\mu\text{m/s}$ using optical tweezers. After reaching the expected initial displacement, we release the force applied on the bead by turning off the laser power, subsequently recording the movement of the released bead by microscopic imaging. After releasing the loading force, the bead moves backward with time (Fig. 2D–F), indicating an elastic recovery of the cytoplasmic deformation. We find that there is full recovery of deformations up to $X/a = 0.8$ in WT mEFs, while the $Vim^{-/-}$ mEFs begin to exhibit plastic deformation (i.e., not fully recovered) for deformations X/a below 0.4. This result shows that VIF networks can increase the yielding strain and thus the resilience of the cytoplasm, providing living cells with a mechanism for recovering their original shapes and structures after large deformations.

Hyperelastic VIF Networks Regulate the Toughness of the Cytoplasm by Increasing Both Dissipated Energy and Elastic Energy under Loading. The capacity of energy absorption is an important parameter characterizing materials; it can be quantified using the material's toughness, obtained by calculating the extension work via integrating the stress–strain curve (25). To determine this parameter in cells and to further define the functions of VIF, we have integrated the normalized force–displacement curve to $X/a = 1.2$ to obtain the extension work of cells (Fig. 1I). We find that the extension work is larger in the WT mEFs than the sum of those in the $Vim^{-/-}$ mEFs and the VIF ghost cell (*SI Appendix, Fig. S8*). Since we locally deform the cytoplasm using a bead, complete fracture of the cytoplasm is not achieved at the end of the loading; nevertheless, this comparison suggests that the cytoplasmic toughness of the WT mEFs is greater than the superposition of the $Vim^{-/-}$ mEFs and the VIF ghost cell, indicating a direct interaction between VIFs and the rest of the cytoplasmic components.

To further investigate the underlying mechanisms by which VIFs enhance the toughness and resilience of the cytoplasm, cyclic loading and unloading tests are carried out in cells (Fig. 3A, *Inset*). This test quantifies both the elastic and dissipated mechanical energy that together constitute material toughness. Surprisingly, the loading and unloading curves obtained in the VIF ghost cell collapse and remain unchanged over more than 100 cycles (Fig. 3A). This result further demonstrates that the cytoplasmic VIF network itself is hyperelastic and with negligible

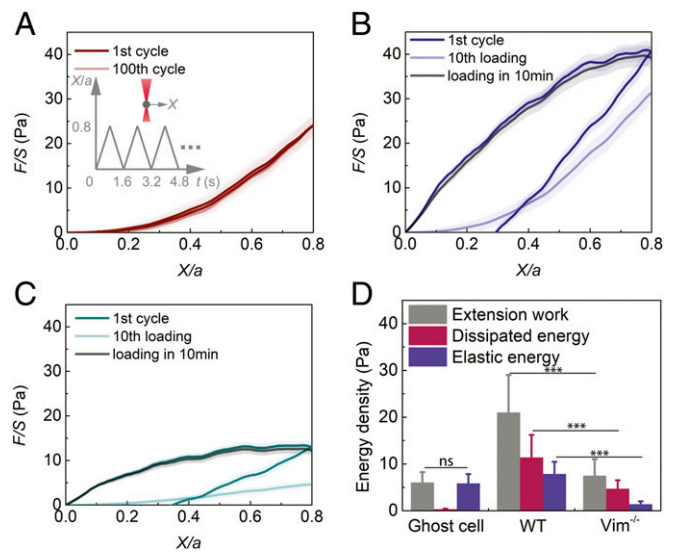


Fig. 3. The VIF network increases the toughness of the cytoplasm by increasing dissipated energy and elastic energy. (A) Cyclic loading in the cell is achieved by reciprocating movement of a bead at a speed of 1 $\mu\text{m/s}$ using optical tweezers (*Inset*). The first and 100th loading and unloading curves in VIF ghost cells overlap. The semitransparent band around the average curves represents the SE ($n = 15$ cells). (B and C) Plot of the first and 10th cyclic loading curves in WT mEFs (B) and $Vim^{-/-}$ mEFs (C). After being damaged by repeated loadings, the loading curves in both WT and $Vim^{-/-}$ mEFs recover to original levels in 10 min, highlighting the self-healing nature of the cytoplasm. The semitransparent band around the average curves represents the SE ($n = 20$ cells for each curve). See full curves in *SI Appendix, Fig. S10*. (D) VIF ghost cell does not dissipate energy. WT mEFs have significantly higher extension work, dissipated energy, and elastic energy than $Vim^{-/-}$ mEFs. Error bars represent SD ($n = 15$ cells for ghost cells, $n = 20$ cells for WT and $Vim^{-/-}$ mEFs). ns, not significant; *** $P < 0.001$.

energy dissipation (Fig. 3D). Individual VIFs have been shown to be capable of dissipating mechanical energy due to unfolding of α helices under stretch on single filaments (26–28); our results suggest that before individual filaments reaching this unfolding state, the VIF networks could globally retain an elastic regime under moderate to large deformations. When this measurement is made in the WT mEFs, a clear hysteresis loop is observed, suggesting energy is being dissipated during this process (Fig. 3B and *SI Appendix, Fig. S10*). Furthermore, the cytoplasm is greatly softened over the first 3 cycles and eventually becomes similar to that measured in the ghost cell after 10 cycles (Fig. 2B and *SI Appendix, Fig. S10*). In contrast, the resistant force in the $Vim^{-/-}$ mEFs eventually becomes very weak (Fig. 3C), suggesting that cyclic loading causes most cytoskeletal structures to be damaged, disassembled, or rearranged in cells without VIFs. After repeated cyclic loading, the normalized force–displacement curve reaches a steady state at the 10th cycle in both WT and $Vim^{-/-}$ mEFs; integration of the steady-state force–displacement curve represents the elastic energy of the cytoplasm. These results show that elastic energy is significantly higher in the WT mEFs as compared to the $Vim^{-/-}$ mEFs (Fig. 3D), further suggesting that the VIF network maintains the resilience of the cytoplasm during cyclic loading, while the rest of the cytoplasmic components (such as F-actin and microtubules) contribute to the energy dissipation. To further quantify the energy dissipation, we integrate the area looped by the first loading and unloading curves (Fig. 3A–C). We find that the dissipated energy density is significantly higher in the WT mEFs than in the $Vim^{-/-}$ mEFs (Fig. 3D), demonstrating that the existence of the VIF network can also substantially increase the energy dissipated by the cytoplasm. Since the VIF network itself is hyperelastic and

does not dissipate mechanical energy (Fig. 3D), the observed enhancement in energy dissipation is more likely due to other cellular components (F-actin, MTs, and cytosol) through their interactions with VIFs. Therefore, the stretchy elastic VIF network and the other dissipative cytoplasmic components work synergistically, enhancing cytoplasmic toughness. Indeed, the VIF network interpenetrates with other cytoskeletal networks as shown in previous literature (29, 30), providing an unavoidable physical interaction between different networks.

Our results show that VIFs are essential for the cytoplasm to retain high strength, stretchability, and toughness under frequent large deformations, thus preventing the cytoplasm from becoming irreversibly damaged during important cell migratory and invasive activities. Interestingly, we also find that the living cytoplasm shows significant softening after repeated loading but can recover to its original state after a 10-min rest (Fig. 3 B and C). This likely reflects the rapid self-reorganizing ability of other cytoskeletal structures, as also observed in both mechanical testing and microscopic imaging of reconstituted actin and microtubule networks (31–34), even though these 2 cytoskeletal structures are easily disassociated upon initial loading. Such mechanically recovering after damage observed in the living cell cytoplasm is substantially more efficient than in typical artificial materials (35).

Hyperelastic VIF Networks Extend the Cytoplasmic Deformation Field under Localized Loading. To further understand the mechanisms by which VIFs enhance and regulate the mechanical properties of cytoplasm and increase the dissipated mechanical energy of the cytoplasm, we image the resultant displacement and strain fields upon introducing a local deformation in the cytoplasm. We drag a 2- μm -diameter bead in the cytoplasm over 200 nm at a speed of 2 $\mu\text{m/s}$ and perform particle image velocimetry by visualizing 2D projected movements of surrounding fluorescently labeled mitochondria (Fig. 4 A and B). We find that the deformation field extends significantly farther in the WT mEFs than in the *Vim*^{-/-} mEFs (Fig. 4 C and D and [Movies S2](#) and [S3](#)). To quantify this effect, we plot the local cytoplasmic displacement as a function of the distance to the loading center along the drag direction (white dashed lines in Fig. 4 C and D), where the

displacement (U) is normalized by the bead displacement (U_0), and the distance (X) is normalized by the bead radius (R), as shown in Fig. 4G. The normalized displacement decays with normalized distance as a power law with a power of -1 in the cytoplasm of the WT mEFs. In contrast, the observed displacement decay is markedly faster in the *Vim*^{-/-} mEFs (Fig. 4G) with a power of -2 . Consistently, the normal strain field computed from the 2D displacement map concentrates around the loading point in the *Vim*^{-/-} mEFs while it extends significantly farther in the WT mEFs (Fig. 4 E and F and [SI Appendix, Fig. S11](#)). To further show that VIFs dominate the deformation fields, we perform this measurement in VIF overexpression mEFs ([SI Appendix, Fig. S7](#)) and WT mEFs with F-actin and MTs depolymerized ([SI Appendix, Fig. S6](#)); we do not observe any statistically significant difference in the deformation field in either of these cells, as compared to the control WT mEFs. Taken together, these results demonstrate the important contribution of VIF networks in increasing the propagation of local deformations in the cytoplasm, therefore involving more cytoplasmic materials to deform under to local loading.

Other cytoskeletal components such as F-actin and microtubules are easily relaxed and reorganized under deformation, as shown by both our measurements in cells (Fig. 24) and macroscopic rheology measurements of reconstituted networks (21); once relaxed and reorganized, they quickly lose the ability to transmit stress and strain. However, the high stretchability and hyperelastic nature of the VIF network allows it to maintain structural and mechanical integrity under very large strains (more than 300%), therefore enabling local strain and stress to be effectively transmitted from a stress concentrated area to a larger zone in the cell (Fig. 4H). As widely observed in common materials, stress/strain concentrations are the major cause of material damage (36). Under a concentrated loading, the stretchy, hyperelastic VIF network not only stores substantial mechanical energy by itself but also increases the dissipated mechanical energy significantly by deforming larger volumes of the cytoplasm near the stress concentration. Therefore, the presence of such an interconnected VIF network can markedly increase the required mechanical energy to damage the cytoplasm under the same loading force.

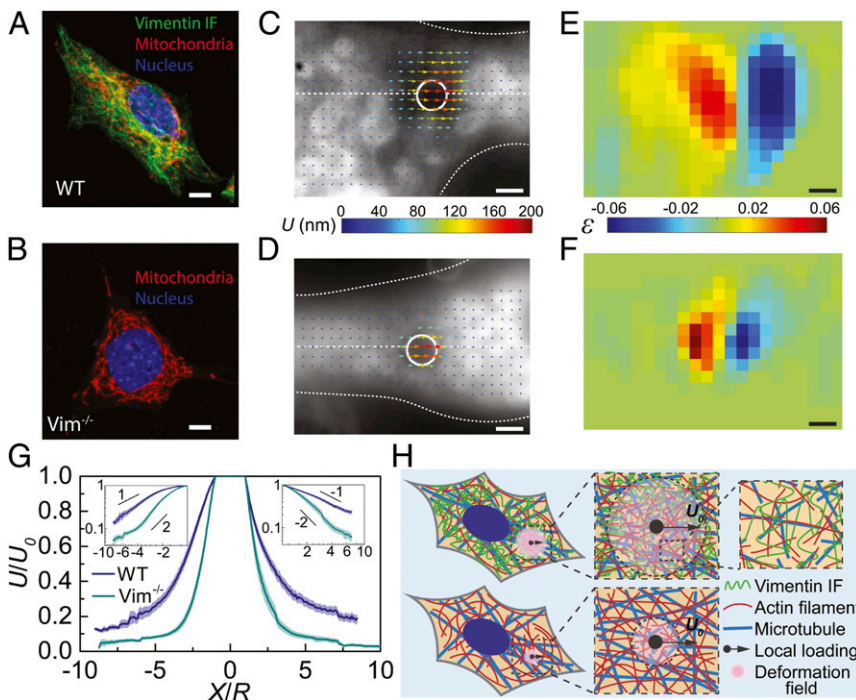


Fig. 4. VIFs extend the cytoplasmic deformation field under local loading, acting as a stretchable hyperelastic network. (A and B) Deformation field is obtained by dragging a 2- μm -diameter bead in the cytoplasm over 200 nm and visualizing the 2D projected movements of surrounding fluorescently labeled mitochondria. (C and D) The displacement fields around the loading beads (white circle) in WT and *Vim*^{-/-} mEFs (cell boundaries are marked with white dotted lines). The color and the length of arrows represent displacement magnitudes. (E and F) The normal strain fields in WT and *Vim*^{-/-} mEFs are obtained from displacement fields shown in C and D. The color represents the magnitude of normal strain. (G) Plot of the normalized cytoplasmic displacement as a function of the normalized distance to the loading center, along the drag directions (horizontal white dashed lines in C and D). Log-log plots are shown in the *Insets*. The semitransparent band around the average curves represents the SE ($n = 15$ cells for each curve). (H) Schematics to illustrate the mechanism of extending deformation fields by VIF network. Highly stretchable VIF networks maintain the elasticity of and transmit local strain through a large zone in the cytoplasm, while other cytoskeletal structures are easy to be damaged under deformation. The cytoskeletal mesh size and bead size are not in their actual proportion, just for illustration. (Scale bars: 10 μm in A and B and 2 μm in C–F.)

Discussion

This work uncovers the essential role of VIFs in cell mechanical behavior under large deformations. As a highly stretchable hyperelastic network, the cytoskeletal VIF network greatly enhances several of the most important mechanical properties of the cytoplasm: stretchability, resilience, strength, and toughness (SI Appendix, Table S1). The cytoplasmic stretchability is mainly determined by the VIF network. Subjected to repeated loadings, the VIF network plays an essential role in maintaining the resilience of the cytoplasm because of its high yielding strain, while the rest of cytoplasmic components are greatly softened or even disassembled. By interacting with other cytoskeletal systems and organelles, VIF networks significantly enhance cytoplasmic mechanical strength and toughness under dynamic deformations, through slowing poroelastic and viscoelastic relaxations. Moreover, the stretchy VIF network can effectively propagate local stress and strain into a larger region of the cell, deforming more microtubules and actin filaments which interpenetrate and interact with the VIF network (37, 38). Thus, VIFs significantly enhance the strength and toughness of the cytoplasm, reducing the risk of cell damage during processes involving large deformations. The enhancement of mechanical properties by VIFs is most likely required for mesenchymal cells to perform many physiological activities including cell migration during embryonic development, wound healing, and cancer metastasis. These properties of

the VIF networks may also shed light on the roles of other types of intermediate filament networks, as well as on the pathogenesis of the many human diseases associated with mutations in IF-encoding genes (39, 40). Furthermore, the stretchy and hyperelastic VIF network forms a dynamic yet mechanically robust cytoskeleton when combined with the dissipative and quickly recovering cytoskeletal components such as microtubules and actin filaments; such a collaborative design principle may inspire improved engineering of smart materials.

Materials and Methods

Full materials and methods are described in SI Appendix. Briefly, to investigate the mechanical property of the living mammalian cytoplasm, we deliver micrometer-sized polystyrene beads into living mouse embryonic fibroblasts through endocytosis. These beads distribute randomly inside the cell. To obtain the force–displacement curve in the cytoplasm, we use optical tweezers to trap and pull a bead unidirectionally with a constant speed (19, 41). To avoid any interactions with the mechanically distinct cell cortex and nucleus, we only use beads that are positioned greater than 1.5 μm away from the cell boundary and away from both the thin lamellar region and the nucleus (11, 16, 19).

ACKNOWLEDGMENTS. We thank P. Ronceray, Y. Zheng, and the M.G. laboratory for helpful discussions. This work is supported by National Cancer Institute Grant 1U01CA202123. S.C. acknowledges support from Hellman Fellows Fund. H.W. and R.D.G. acknowledge the support from the National Institutes of Health (Grant 2P01GM096971-06A1).

- R. Kalluri, EMT: When epithelial cells decide to become mesenchymal-like cells. *J. Clin. Invest.* **119**, 1417–1419 (2009).
- J. Yang, R. A. Weinberg, Epithelial-mesenchymal transition: At the crossroads of development and tumor metastasis. *Dev. Cell* **14**, 818–829 (2008).
- A. Mantovani, Cancer: Inflaming metastasis. *Nature* **457**, 36–37 (2009).
- C. M. Denais *et al.*, Nuclear envelope rupture and repair during cancer cell migration. *Science* **352**, 353–358 (2016).
- M. Raab *et al.*, ESCRT III repairs nuclear envelope ruptures during cell migration to limit DNA damage and cell death. *Science* **352**, 359–362 (2016).
- D. A. Fletcher, R. D. Mullins, Cell mechanics and the cytoskeleton. *Nature* **463**, 485–492 (2010).
- P. A. Janmey, U. Euteneuer, P. Traub, M. Schliwa, Viscoelastic properties of vimentin compared with other filamentous biopolymer networks. *J. Cell Biol.* **113**, 155–160 (1991).
- O. I. Wagner *et al.*, Softness, strength and self-repair in intermediate filament networks. *Exp. Cell Res.* **313**, 2228–2235 (2007).
- E. Latorre *et al.*, Active superelasticity in three-dimensional epithelia of controlled shape. *Nature* **563**, 203–208 (2018).
- M. G. Mendez, S. Kojima, R. D. Goldman, Vimentin induces changes in cell shape, motility, and adhesion during the epithelial to mesenchymal transition. *FASEB J.* **24**, 1838–1851 (2010).
- M. Guo *et al.*, The role of vimentin intermediate filaments in cortical and cytoplasmic mechanics. *Biophys. J.* **105**, 1562–1568 (2013).
- N. Wang, D. Stamenović, Contribution of intermediate filaments to cell stiffness, stiffening, and growth. *Am. J. Physiol. Cell Physiol.* **279**, C188–C194 (2000).
- M. G. Mendez, D. Restle, P. A. Janmey, Vimentin enhances cell elastic behavior and protects against compressive stress. *Biophys. J.* **107**, 314–323 (2014).
- S. Hong *et al.*, 3D printing of highly stretchable and tough hydrogels into complex, cellularized structures. *Adv. Mater.* **27**, 4035–4040 (2015).
- K. Luby-Phelps, “Cytoarchitecture and physical properties of cytoplasm: Volume, viscosity, diffusion, intracellular surface area” in *International Review of Cytology*, H. Walter, D. E. Brooks, P. A. Srere, Eds., (Elsevier, 1999), vol. 192, pp. 189–221.
- M. Guo *et al.*, Probing the stochastic, motor-driven properties of the cytoplasm using force spectrum microscopy. *Cell* **158**, 822–832 (2014).
- S. K. Gupta, M. Guo, Equilibrium and out-of-equilibrium mechanics of living mammalian cytoplasm. *J. Mech. Phys. Solids* **107**, 284–293 (2017).
- M. Guo *et al.*, Cell volume change through water efflux impacts cell stiffness and stem cell fate. *Proc. Natl. Acad. Sci. U.S.A.* **114**, E8618–E8627 (2017).
- J. Hu *et al.*, Size- and speed-dependent mechanical behavior in living mammalian cytoplasm. *Proc. Natl. Acad. Sci. U.S.A.* **114**, 9529–9534 (2017).
- S. Sivaramakrishnan, J. V. DeGiulio, L. Lorand, R. D. Goldman, K. M. Ridge, Micro-mechanical properties of keratin intermediate filament networks. *Proc. Natl. Acad. Sci. U.S.A.* **105**, 889–894 (2008).
- C. Storm, J. J. Pastore, F. C. MacKintosh, T. C. Lubensky, P. A. Janmey, Nonlinear elasticity in biological gels. *Nature* **435**, 191–194 (2005).
- B. Fabry *et al.*, Scaling the microrheology of living cells. *Phys. Rev. Lett.* **87**, 148102 (2001).
- E. Moeendarbary *et al.*, The cytoplasm of living cells behaves as a poroelastic material. *Nat. Mater.* **12**, 253–261 (2013).
- M. Balland *et al.*, Power laws in microrheology experiments on living cells: Comparative analysis and modeling. *Phys. Rev. E Stat. Nonlin. Soft Matter Phys.* **74**, 021911 (2006).
- J.-Y. Sun *et al.*, Highly stretchable and tough hydrogels. *Nature* **489**, 133–136 (2012).
- J. Block *et al.*, Viscoelastic properties of vimentin originate from nonequilibrium conformational changes. *Sci. Adv.* **4**, eaat1161 (2018).
- Z. Qin, L. Kreplak, M. J. Buehler, Hierarchical structure controls nanomechanical properties of vimentin intermediate filaments. *PLoS One* **4**, e7294 (2009).
- J. Block *et al.*, Nonlinear loading-rate-dependent force response of individual vimentin intermediate filaments to applied strain. *Phys. Rev. Lett.* **118**, 048101 (2017).
- C. Leduc, S. Etienne-Manneville, Intermediate filaments in cell migration and invasion: The unusual suspects. *Curr. Opin. Cell Biol.* **32**, 102–112 (2015).
- R. D. Goldman, D. M. Knipe, “Functions of cytoplasmic fibers in non-muscle cell motility” in *Cold Spring Harbor Symposia on Quantitative Biology* (Cold Spring Harbor Laboratory Press, 1973), pp. 523–534.
- T. P. Loisel, R. Boujemaa, D. Pantaloni, M.-F. Carlier, Reconstitution of actin-based motility of *Listeria* and *Shigella* using pure proteins. *Nature* **401**, 613–616 (1999).
- B. Vitre *et al.*, EB1 regulates microtubule dynamics and tubulin sheet closure in vitro. *Nat. Cell Biol.* **10**, 415–421 (2008).
- O. Chaudhuri, S. H. Parekh, D. A. Fletcher, Reversible stress softening of actin networks. *Nature* **445**, 295–298 (2007).
- F. J. Nédélec, T. Surrey, A. C. Maggs, S. Leibler, Self-organization of microtubules and motors. *Nature* **389**, 305–308 (1997).
- D. L. Taylor, M. In Het Panhuis, Self-healing hydrogels. *Adv. Mater.* **28**, 9060–9093 (2016).
- P. Weißgraber, D. Leguillon, W. Becker, A review of finite fracture mechanics: Crack initiation at singular and non-singular stress raisers. *Arch. Appl. Mech.* **86**, 375–401 (2016).
- Z. Gan *et al.*, Vimentin intermediate filaments template microtubule networks to enhance persistence in cell polarity and directed migration. *Cell Syst.* **3**, 252–263.e8 (2016).
- N. Costigliola *et al.*, Vimentin fibers orient traction stress. *Proc. Natl. Acad. Sci. U.S.A.* **114**, 5195–5200 (2017).
- E. Fuchs, K. Weber, Intermediate filaments: Structure, dynamics, function, and disease. *Annu. Rev. Biochem.* **63**, 345–382 (1994).
- F. Danielsson, M. K. Peterson, H. Caldeira Araújo, F. Lautenschläger, A. K. B. Gad, Vimentin diversity in health and disease. *Cells* **7**, E147 (2018).
- Y. L. Han *et al.*, Cell contraction induces long-ranged stress stiffening in the extracellular matrix. *Proc. Natl. Acad. Sci. U.S.A.* **115**, 4075–4080 (2018).